

Nearly degenerate ground states of a checkerboard antiferromagnet and their bosonic interpretation

Haiyuan Zou (邹海源),^{1,*} Fan Yang (杨帆),² and Wei Ku (顧威)^{1,3,†}

¹*Tsung-Dao Lee Institute & School of Physics and Astronomy,
Shanghai Jiao Tong University, Shanghai 200240, China*

²*Department of Physics, Beijing Institute of Technology, Beijing 100081, China*

³*Key Laboratory of Artificial Structures and Quantum Control (Ministry of Education), Shanghai 200240, China*

The spin-1/2 model system with antiferromagnetic (AF) couplings on a J_1 - J_2 checkerboard lattice, known as the planar pyrochlore model, is strongly frustrated and associate with a two-to-one dimensional (2D-to-1D) crossover. Using the Projected Entangled Simplex States tensor network ansatz, we identify several nearly degenerate states in the frustrated region ($J_1 < J_2$). Specifically, we find the long-sought crossed-dimer valence bond solid (VBS) state to be the ground state at $J_1 \lesssim J_2$, while 1D AF correlated states take over the rest. We verify the stability of the VBS state against nematic perturbation. The corresponding bosonic picture provides an intuitive understanding of the low-energy physics. Particularly, it predicts a weaker VBS states in the easy-plane limit, which we confirm numerically. Our results clarify the most essential question of this interesting system, and demonstrate the usefulness of bosonic picture in dealing with frustrated magnetism.

Determining the many-body ground states and classifying the phase transitions in strongly correlated systems are two central quests of condensed matter physics. For these purposes, physicists are interested in the low-dimensional frustrated systems which defeat long-range orders and exhibit exotic paramagnetic ground states such as the quantum valence bond solid (VBS) [1] and the spin liquid [2–4]. Meanwhile, the past few decades witness the fast development of quantum fluctuation driven phase transition [5–7] beyond the conventional Landau’s symmetry-broken mechanism. Exploring the nature of frustrated systems and the associated quantum phase transition might give valuable insights to the understanding of the high temperature superconductivity [8] and the realization of quantum computing [9]. Realistically, frustration is induced by the combing effects from nontrivial lattice geometries [10], competition of couplings [11], and exotic interactions [12]. Although great theoretical progress and fast development of many techniques have been made, the nature of the ground state of many frustrated systems still remains controversial [13–18]. It is important to consider these problems from a different angle.

The antiferromagnetic (AF) spin-1/2 model on a two-dimensional (2D) checkerboard lattice, also known as the planar pyrochlore model, is a paradigmatic example with a highly frustrated interactions. It is described by the Hamiltonian:

$$H = J_1 \sum_{\text{NN}} \mathbf{S}_i \cdot \mathbf{S}_j + J_2 \sum_{\text{NNN}} \mathbf{S}_i \cdot \mathbf{S}_k, \quad (1)$$

where \mathbf{S}_i is the spin operator on site i , $J_{1,2}$ are the exchange couplings between the spins with the nearest neighbors (NN) and the next nearest neighbors (NNN), respectively. At $J_1 \gg J_2$, the system has a ground state with 2D AF correlation along J_1 bonds (cf: red bands in

Fig. 1), leaving a strongly ferromagnetic correlation along

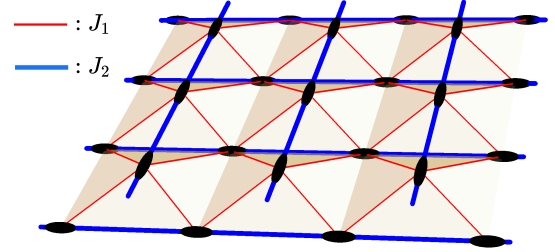


FIG. 1. Planar pyrochlore model in the 1D dominant region. Lattice sites (ovals) are coupled along the 1D chain via the stronger J_2 (blue) bonds, followed by weaker 2D coupling along the J_1 (red) bonds.

the J_2 (blue) bonds. At the opposite limit $J_2 \gg J_1$, the system reduced to one-dimensional (1D) AF correlated chains along the J_2 (blue) bonds weakly coupled by geometric frustrated J_1 interaction, drastically incompatible with the 2D limit. The corresponding ground state is believed to be a sliding Luttinger liquid [19]. Thus, the system hosts a 2D-to-1D crossover reflecting the severe competition between these two interactions.

This frustrated system with the dimensional crossover feature has attracted tremendous studies with different techniques [7, 19–23, 25]. In the region of $J_2 \sim J_1$, it is believed that the ground state is a plaquette-VBS (P-VBS) state [20–22]. However, the true ground state at $J_2 > J_1$ is still under serious debate. An earlier proposal [23] suggested a crossed-dimer type VBS (CD-VBS) state, which was indirectly supported by the coupled cluster method [25]. On the other hand, tensor network with Projected Entangled Pair States ansatz found a stripe ordered phase instead [7]. In addition, the nature of the phase transitions between these different possible ground states are still at large [23].

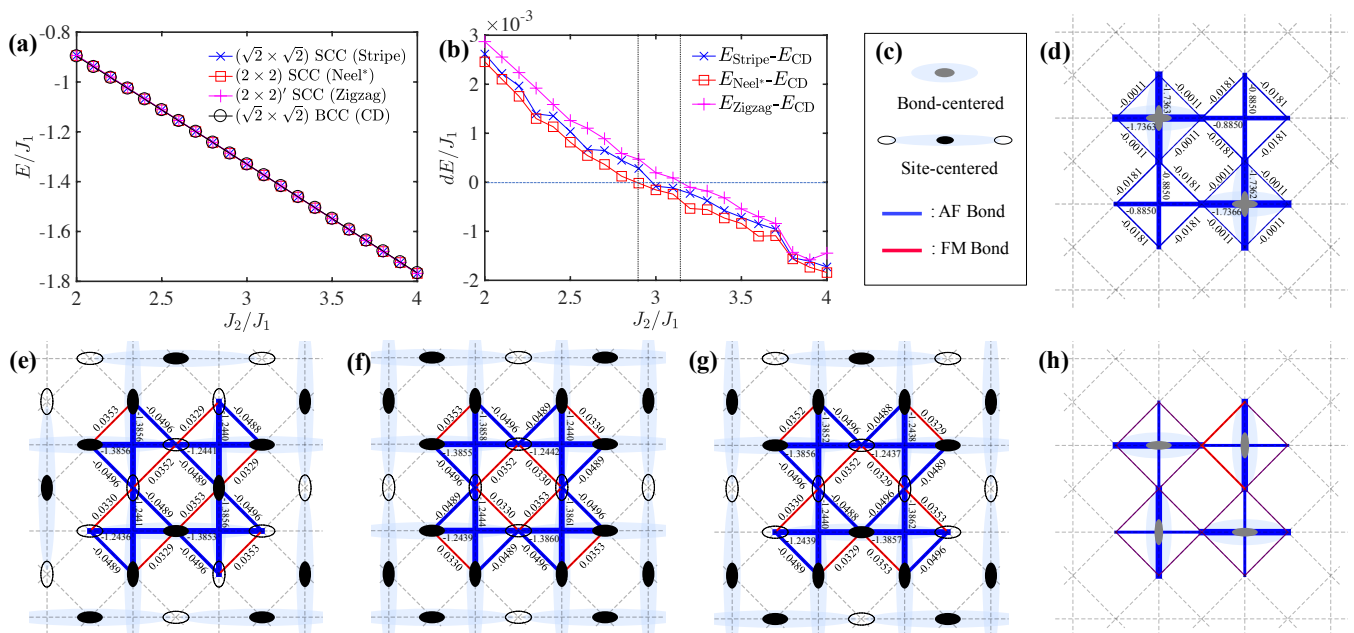


FIG. 2. (a) Energies of nearly degenerate states as functions of $J_2 > J_1$. (b) The same using the CD (BCC) state as a reference, showing that the CD (BCC) state becomes the ground state below the region around $J_2 \sim 3J_1$ (between two vertical dotted lines). (c) Illustration of the spread of the bosonic orbitals in BCC and SCC states in panels (d-h), in which blue and red lines demote AF and FM bonds. (d-g) Examples of the bond energies in various nearly degenerate states corresponding to different bosonic charge correlations at $J_2/J_1 = 3$ in a 2×2 PESS unit cell: (d) $(\sqrt{2} \times \sqrt{2})$ BCC (crossed-dimer), (e) $(\sqrt{2} \times \sqrt{2})$ SCC (stripe), (f) (2×2) SCC (Néel*), and (g) $(2 \times 2)'$ SCC (zigzag). (h) An example of higher energy states, in which the two red bonds connect to the same dimer and thus can only benefit limited kinetic energy lowering.

One should, however, be cautious about detailed results from the tensor network methods [1, 8, 26, 27, 29–33, 35], as the dominant quantum entanglement of the states are directly affected by the particular ansatz employed in the implementation, in addition to the control parameter “virtual bond dimension”. Consequently, the best choice of ansatz is highly dependent on the specific geometrical structure of the system [1, 36].

Here, using a recent developed tensor network ansatz, i.e., the projected entangled simplex states (PESS) [1] in the thermodynamic limit, we obtain multiple nearly degenerate ground states in the $J_1 < J_2$ region, including the long-sought CD-VBS state. The near degeneracy of these states explains why the ground state is elusive in previous studies, and demonstrates the superiority of PESS in capturing both 1D and 2D entanglement of this system [1, 37]. Specifically, while 1D AF correlated states is slightly lower in energy for $J_1 \ll J_2$, the CD-VBS state becomes the ground state at $J_1 \lesssim J_2$. We further confirm the stability of CD-VBS state by exposing it to a nematic perturbation. An intuitive understanding for these states emerges through different local charge correlations in a bosonic picture, which helps elucidate the nature of the phase transitions. The picture also points out a slight disadvantage of the 1D AF correlated states due to the effective repulsion. We verify this analysis by showing

a smaller CD-VBS region in the easy-plane limit (XY -limit) of the model. Interestingly, at the $J_1 \gtrsim J_2$ we not only find the known P-VBS state, but also find a surprising out-of-plane spin-configuration in the XY -limit, corresponding to a bosonic charge-density-wave (CDW). Our results solve the ground state question of this fascinating system, and exhibit a useful bosonic picture for frustrated magnetism.

We use a 2×2 (with a J_2 bond as one lattice spacing) PESS [1] unit cell which contains eight different local tensors to explore the checkerboard AF model (Eq. 1). The size of the unit cell (i.e.: the size of translational unit in spontaneously symmetry broken states) turns out to be an important ingredient in our thermodynamic limit calculation. We found that a “virtual bond dimension” $D = 4$ already reach lower energies than other methods [37].

Figure 2(a) shows nearly identical energy for different states at $J_2 > J_1$ found in our calculation. Particularly, for the first time we find the direct evidence of a CD-VBS state [23] [Fig. 2(d)], in addition to the stripe state [Fig. 2(e)] and Néel* state [Fig. 2(f)]. Surprisingly, a new zigzag state with a 2×2 period [labeled as $(2 \times 2)'$ in [Fig. 2(g)] also appears in our calculation. All (e)-(g) are similar 1D AF correlated states different from the CD-VBS state due to qualitatively distinct entanglements.

To better understand these states, we find it is very helpful to employ a bosonic picture. Using the fully down-spin polarized state as a reference, the local spin state can be represented by a hard-core boson, b^\dagger with $b_i^\dagger b_i^\dagger = 0$, through $S_i^+ \rightarrow b_i^\dagger$, $S_i^- \rightarrow b_i$, and $S_i^z \rightarrow n_i - 1/2$ ($n_i \equiv b_i^\dagger b_i$). Table I translates the most relevant physics of our spin system into the bosonic picture. Intuitively, the AF Ising coupling $S_i^z S_j^z$ becomes an effective repulsion between two bosons or two holes, disfavoring parallel alignment of neighboring spins. Most importantly, the spin-fluctuation $S_i^x S_j^x + S_i^y S_j^y$ conveniently becomes the kinetic energy of a boson, and correspondingly the two-body spin-singlet state is merely a single-particle anti-bonding bosonic state. Such a reduction from a two-body physics to a single-particle one provides a significant simplification in systems with strong fluctuation in general.

| Spin picture | Bosonic picture |
|---|--|
| $S_i^x S_j^x + S_i^y S_j^y$ | $b_i^\dagger b_j + b_j^\dagger b_i$ (kinetic energy) |
| $S_i^z S_j^z$ | $(n_i - 1/2)(n_j - 1/2)$ (repulsion) |
| $\frac{1}{\sqrt{2}}(\uparrow\downarrow\rangle - \downarrow\uparrow\rangle)$ | $\frac{1}{\sqrt{2}}(10\rangle - 01\rangle)$ (anti-bonding) |

TABLE I. The spin and boson correspondence.

For example, in our AF checkerboard lattice, the lack of global magnetization implies that our bosonic system should generally be half-filled, making them easily stuck into some sort of local charge order. The larger $J_2 b_i^\dagger b_j$ dictates an alternating charge order along the J_2 direction for low-energy states, such that each boson has a chance to extend its orbital to lower its kinetic energy. Next, the smaller $J_1 b_i^\dagger b_j$ would similarly prefer to leak into as many empty J_1 -neighbors as possible.

We now demonstrate that this framework provides a very intuitive understanding of the low-energy states of the systems. First, it is easy to understand the nearly identical energies of the 1D AF correlated states in Fig. 2(e)-(g). These states correspond to various site-centered charge correlated (SCC) bosonic states, in which each boson is surrounded by two unoccupied sites along the J_2 and J_1 directions, allowing its orbital to extend and in turn lowering its kinetic energy. In fact, one can easily verify that these are the only SCC ones in our unit cell that satisfy the above considerations [38]. Similarly, the long-sought CD-VBS state also corresponds to a charge correlated state, except that each boson now resides in a bond-centered anti-bonding orbital. It turns out that while such a bond-centered charge correlated (BCC) state has a very different bosonic orbital, its energy can be quite similar to those SCC states. As a counter example, consider a similar BCC state in Fig. 2(h) that also respects the charge correlation along the J_2 directions and therefore might be another candidate of low-energy states. Upon more careful analysis, one finds that the neighboring J_1 hoppings are always

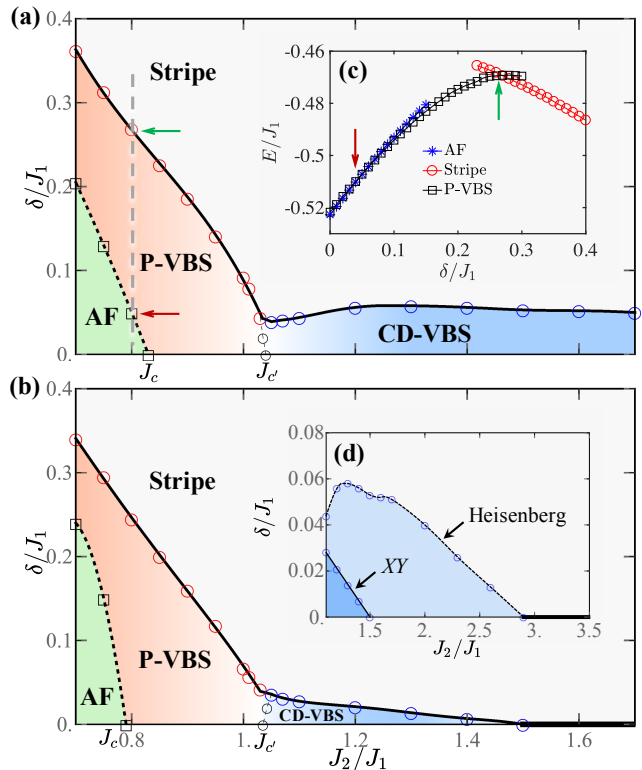


FIG. 3. δ - J_2 phase diagrams of the model in (a) the Heisenberg limit and (b) the XY-limit, demonstrating AF (green), P-VBS (red), CD-VBS (blue), and stripe (grey) phases. Panel (c) illustrates energies of the most competitive states as a function of δ along the grey long dashed line at $J_2 = 0.8J_1$, which indicates a strong (green arrow) and weak (red arrow) first-order transitions. Correspondingly, the solid and dotted lines in (a)&(b) denote phase boundaries of strong and weak first order transitions, respectively. Panel (d) shows that in the XY-limit, the CD-VBS phase starts at a lower value of J_2/J_1 , above which multiple nearly degenerate SCC states take over, denoted by the thick solid lines

partially blocked because each end of the anti-bonding orbital couples to both ends of another orbitals through J_1 . In comparison in case (d), half of the J_1 hoppings connects one end of the anti-bonding orbital to only one end of another orbital, allowing some freedom for them to leak into each others as long as their charge fluctuations are correlated. This explains why case (h) is of higher energy and thus unstable in our numerical calculation. We anticipate the usefulness of such a bosonic picture to extend to other frustrated spin systems with nearly degenerate states [39].

The near degeneracy between the CD-VBS and SCC states is not expected to persist in the $J_1 \rightarrow 0$ limit, where the pure 1D solution is exactly known [40] to have only weak dimerization in terms of the bond energy, similar to those in the SCC states. This is not too surprising as these two sets of states are quite different in their bosonic orbital structure discussed above, SCC having

a larger extent of the orbital along the J_2 directions as shown in Fig. 2(c). Indeed, Fig. 2(b) shows that the energy of the CD-VBS state approaches the latter in the vicinity of $J_2 \sim 3J_1$. In fact, CD-VBS state becomes the ground state near $J_1 \lesssim J_2$ due to its avoidance of energy cost associated with the frustrated J_1 bond (blocked bosonic kinetic process) present in the 1D AF states [c.f.: red bonds in Fig. 2(e)-(g)].

One can examine the stability of the CD-VBS state by lowering the energy of the stripy SCC state in Fig. 2(e) via introduction of NN bond anisotropy $\delta = J_1 - J'_1 > 0$, with directions of J'_1 and J_1 are perpendicular to each other. Figure 3(a)&(d) give the resulting phase diagram with a large region of CD-VBS state under weak anisotropy. The finite region of the VBS state confirms that it is indeed a stable ground state at $J_2/J_1 \lesssim 3$ in our calculation.

Upon careful examination of these nearly degenerate states, we found that SCC states suffer more from the effective J_1 repulsion, as demonstrated by the red bonds in Fig. 2(e)-(g). In contrast owing to its bond-centered nature, the CD-VBS state experiences approximately equal amount of repulsion and attraction, resulting in a nearly decoupled crossed dimer [c.f.: thinnest blue bond in Fig. 2(d)]. Therefore, one should be able to further strengthen the SCC phase by relieving the repulsion, via removal of the $S_i^z S_j^z$ coupling (i.e. the XY-limit).

Indeed, our resulting phase diagram of the XY-limit calculation shown in Fig. 3(b)&(d) confirms this intuition. The energy of SCC state is now more competitive such that the CD-VBS phase shrinks to a much smaller region $J_2/J_1 \lesssim 1.5$. Correspondingly, the amount of anisotropy to destroy the CD-VBS phase is also smaller in this case.

Our results above can provide useful insights to some of the real materials. For example, the pyrochlore material GeCu_2O_4 [41, 42] is estimated to have $J_2/J_1 \sim 6$ [41], well within the SCC phase in our results. The near degeneracy of the SCC states implies that the system is highly susceptible to various weak perturbations in real materials [41–43], and might even induce spontaneous symmetry breaking [41–43] that lower the degree of degeneracy.

Generally, the emergence of VBS like states appears to be a generic feature in the strongly frustrated region in many models. Our above bosonic analysis on the emergence of BCC-type VBS state points out a natural mechanism to explain such a rather generic trend. Typically, AF spin systems correspond to half-filled hardcore bosonic system, which easily gets jammed into a local charge correlated structure. In the absence of strong frustration, the larger size of site-centered orbitals would benefit more from the kinetic energy and thus tend to be the dominant ground states. On the other hand in the presence of strong frustration, bond-centered orbitals, having more space to maneuver collectively, are able to

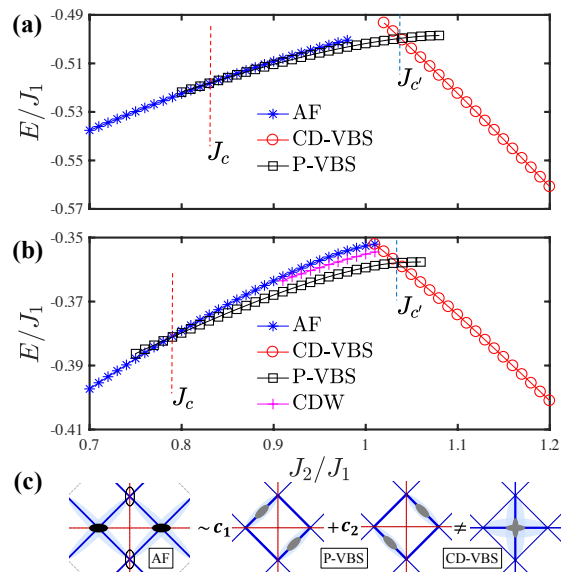


FIG. 4. J_2 -dependent energies of competing states near the quantum phase transitions in the (a) Heisenberg limit and (b) XY-limit for $\delta = 0$, show a weak first-order phase transition at J_c given the similar bosonic orbital structures in (c). In contrast, the transition at $J_{c'}$ is strongly first-order owing to the very different orbital structures in (c) corresponding to the different dominant couplings along J_1 and J_2 bonds. Panel (b) also shows the existence of a meta-stable CDW state containing only out-of-plane spin components.

avoid partially the energy cost of the frustration and thus can eventually take over.

In the 2D checkerboard lattice, another VBS state named P-VBS is known to appear in the 2D dominant ($J_1 \gtrsim J_2$) region (Fig. 3 and Fig. 4). Figure 3 shows that our calculation reproduces this P-VBS state between the 2D AF phase and the stripe phase. Furthermore, Fig. 4(c) demonstrates that the formation of P-VBS state can be understood via the above mechanism as well. In the weakly frustrated region, the ground state is the 2D AF state corresponding to a SCC state with alternating charge along the J_1 directions. As J_2 grows, this state will suffer more and more from the blockage of J_2 paths. Eventually at $J_2/J_1 = J_c \sim 0.8$, the P-VBS will emerge since it is composed of superposition of J_1 -bond-centered orbitals that allow potential kinetic process toward the J_2 directions. This confirms the applicability of the above general picture.

Similar to the 1D dominant region, the SCC 2D AF state has similar energy to the BCC P-VBS state, as shown in Fig. 4. Thus, we anticipate a weak first-order transition at $J_c \sim 0.8$ similar to that at $J_2/J_1 \sim 3$. This result is in agreement with a previous conclusion [23] that deconfined phase transition is highly unlike in this system. In contrast, the change from 2D dominant region ($J_2/J_1 < 1$) to 1D dominant one ($J_2/J_1 > 1$) involves bond-centered orbitals containing different bonds.

One thus expect a strong first-order phase transition at $J_c' \sim 1.04$, supported by the sharp contrast in energy in Fig. 4.

As a side note, in the XY -limit between J_c and J_c' [Fig. 4(b)], we find a unexpected excited state containing an AF correlation that is completely out-of-plane. This state can be understood as a CDW state in the bosonic picture due to enhanced site-centered charge correlation, in associate with the frustration induced suppression of kinetic effects that couple symmetry related degenerate states [37].

In summary, using PESS, a novel tensor network method, we demonstrate several nearly degenerate states in the checkerboard AF system, a prototypical case of magnetically frustrated system hosting a 2D-to-1D dimension crossover. Particularly in the 1D-dominant frustrated region, our calculation produces the long-sought CD-VBS state, which becomes the ground state at $J_2 \gtrsim J_1$. We verify the stability of the VBS state via introduction of a nematic background and find it resilient against a finite strength of nematicity. A simple understanding of our results can be provided by a bosonic picture. The picture also suggests that the CD-VBS state benefits from the charge repulsion (the $S^z S^z$) effect, which we confirm by realizing a weaker CD-VBS state in the XY -limit of the model. Our results resolve a long-standing debate in the active field of quantum frustrated magnetism, and showcase the rich phenomena near quantum phase transition in strongly correlated systems.

ACKNOWLEDGMENTS

We thank Anthony Hegg, Ruizheng Huang, Wei Li, Haijun Liao, Sudeshna Sen, Ling Wang, Rui Wang, Tao Xiang, and Zhiyuan Xie for helpful discussions. This work is supported by National Natural Science Foundation of China (NSFC) #11804221. FY acknowledges supports from NSFC #11674025 and 12074031. WK acknowledges supports from NSFC #11674220 and 11745006 and Ministry of Science and Technology #2016YFA0300500 and 2016YFA0300501.

* wlzouhy@sjtu.edu.cn

† weiku@sjtu.edu.cn

- [1] N. Read and S. Sachdev, Phys. Rev. Lett. **62**, 1694 (1989).
- [2] P. W. Anderson, Science **235**, 1196 (1987).
- [3] L. Savary and L. Balents, Reports on Progress in Physics **80**, 016502 (2016).
- [4] Y. Zhou, K. Kanoda, and T.-K. Ng, Rev. Mod. Phys. **89**, 025003 (2017).
- [5] J. M. Kosterlitz and D. J. Thouless, Journal of Physics C: Solid State Physics **6**, 1181 (1973).
- [6] S. Sachdev, *Quantum Phase Transitions* (2011).
- [7] T. Senthil, L. Balents, S. Sachdev, A. Vishwanath, and M. P. A. Fisher, Phys. Rev. B **70**, 144407 (2004).
- [8] P. A. Lee, N. Nagaosa, and X.-G. Wen, Rev. Mod. Phys. **78**, 17 (2006).
- [9] A. Kitaev, Annals of Physics **303**, 2 (2003).
- [10] H. Diep, *Frustrated spin systems* (World Scientific, 2013).
- [11] P. Chandra and B. Doucot, Phys. Rev. B **38**, 9335 (1988).
- [12] A. Kitaev, Annals of Physics **321**, 2 (2006).
- [13] S. Yan, D. A. Huse, and S. R. White, Science **332**, 1173 (2011).
- [14] Y. Iqbal, F. Becca, S. Sorella, and D. Poilblanc, Phys. Rev. B **87**, 060405 (2013).
- [15] H. J. Liao, Z. Y. Xie, J. Chen, Z. Y. Liu, H. D. Xie, R. Z. Huang, B. Normand, and T. Xiang, Phys. Rev. Lett. **118**, 137202 (2017).
- [16] H.-C. Jiang, H. Yao, and L. Balents, Phys. Rev. B **86**, 024424 (2012).
- [17] S.-S. Gong, W. Zhu, D. N. Sheng, O. I. Motrunich, and M. P. A. Fisher, Phys. Rev. Lett. **113**, 027201 (2014).
- [18] L. Wang, Z.-C. Gu, F. Verstraete, and X.-G. Wen, Phys. Rev. B **94**, 075143 (2016).
- [19] O. A. Starykh, R. R. P. Singh, and G. C. Levine, Phys. Rev. Lett. **88**, 167203 (2002).
- [20] W. Brenig and A. Honecker, Phys. Rev. B **65**, 140407 (2002).
- [21] J.-B. Fouet, M. Mambrini, P. Sindzingre, and C. Lhuillier, Phys. Rev. B **67**, 054411 (2003).
- [22] E. Berg, E. Altman, and A. Auerbach, Phys. Rev. Lett. **90**, 147204 (2003).
- [23] O. A. Starykh, A. Furusaki, and L. Balents, Phys. Rev. B **72**, 094416 (2005).
- [7] Y.-H. Chan, Y.-J. Han, and L.-M. Duan, Phys. Rev. B **84**, 224407 (2011).
- [25] R. F. Bishop, P. H. Y. Li, D. J. J. Farnell, J. Richter, and C. E. Campbell, Phys. Rev. B **85**, 205122 (2012).
- [26] F. Verstraete and J. I. Cirac, (2004), arXiv:cond-mat/0407066.
- [27] J. Jordan, R. Orús, G. Vidal, F. Verstraete, and J. I. Cirac, Phys. Rev. Lett. **101**, 250602 (2008).
- [8] G. Vidal, Phys. Rev. Lett. **98**, 070201 (2007).
- [29] U. Schollwöck, Annals of Physics **326**, 96 (2011).
- [30] R. Orús, Annals of Physics **349**, 117 (2014).
- [31] G. Vidal, Phys. Rev. Lett. **99**, 220405 (2007).
- [32] M. Levin and C. P. Nave, Phys. Rev. Lett. **99**, 120601 (2007).
- [33] Z.-C. Gu, M. Levin, and X.-G. Wen, Phys. Rev. B **78**, 205116 (2008).
- [1] Z. Y. Xie, J. Chen, J. F. Yu, X. Kong, B. Normand, and T. Xiang, Phys. Rev. X **4**, 011025 (2014).
- [35] S. R. White, Phys. Rev. Lett. **69**, 2863 (1992).
- [36] P. Corboz, K. Penc, F. Mila, and A. M. Läuchli, Phys. Rev. B **86**, 041106 (2012).
- [37] See Supplemental Material for detail description.
- [38] The bosonic picture does allow the possibility that more nearly degenerate states might be found with larger PESS unit cell.
- [39] Z. Zhu, D. A. Huse, and S. R. White, Phys. Rev. Lett. **111**, 257201 (2013).
- [40] H. Bethe, Zeitschrift für Physik **71**, 205 (1931).
- [41] T. Yamada, Z. Hiroi, M. Takano, M. Nohara, and H. Takagi, Journal of the Physical Society of Japan **69**, 1477 (2000).
- [42] T. Zou, Y.-Q. Cai, C. R. dela Cruz, V. O. Garlea, S. D. Mahanti, J.-G. Cheng, and X. Ke, Phys. Rev. B **94**,

Supplemental Materials for “Nearly degenerate ground states of a checkerboard antiferromagnet and their bosonic interpretation”

PROJECTED ENTANGLED SIMPLEX STATES TENSOR NETWORKS

We use a recent developed tensor network ground state wave-function ansatz, i.e., the projected entangled simplex states (PESS) [S1], to calculate the ground state of the many-body Hamiltonian (Eq. 1 in the main text) with J_1 and J_2 couplings on a checkerboard lattice. The basic structure of the PESS (shown in Fig. S1) is constructed by the local tensors T with physical indexes σ on each lattice site, the simplex core tensors S on the plaquettes with J_2 bonds, and the bond vectors λ connecting T and S . With all these ingredients, the ground state wave-function can be expressed as

$$|\Psi(\dots\sigma\dots)\rangle = \text{Tr}(\dots T_{lm}^\sigma \lambda_{mn} S_{nij k} \dots) \quad (\text{S1})$$

where i, j, \dots, n are virtual indexes characterizing the quantum entanglement of the system and Tr stands for the contraction of all the virtual indexes.

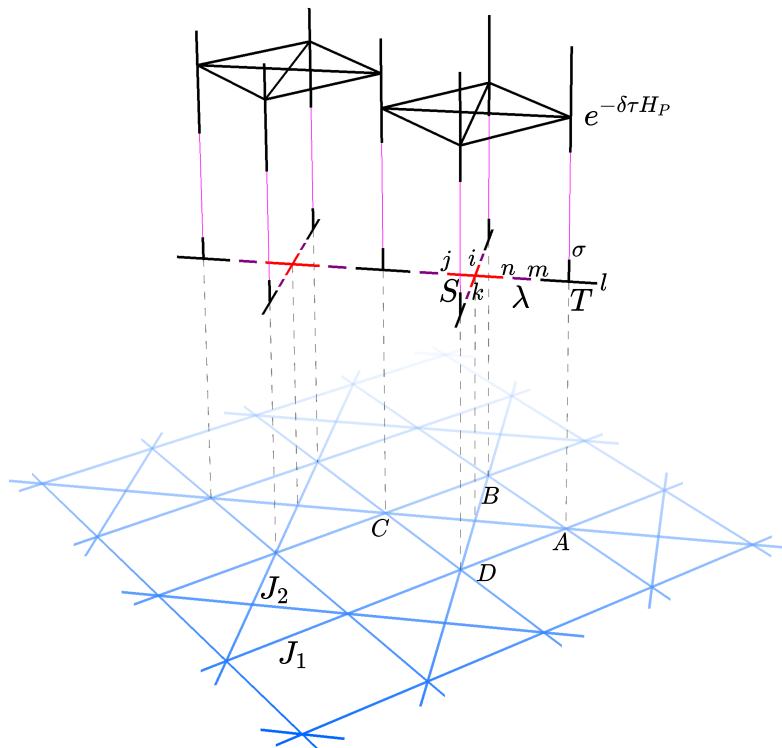


FIG. S1. The J_1 - J_2 model with the nearest (J_1) and the next nearest (J_2) neighbor couplings on a checkerboard lattice is illustrated at the bottom. The ground state is represented by a PESS tensor network in the middle with the local tensors T on the sites, the core tensors S on the plaquettes with J_2 bonds, and the bond vector λ in between of them. On top of the network, a symmetric updating scheme with H_P on each plaquette is chosen to evolve the network to the ground state.

The tensor network wave-function in the thermodynamic limit is constructed by repeating the translational invariant building blocks, i.e., unit cells in both horizontal and vertical directions in 2D. The numbers of the local ingredients T , S , and λ in one unit cell are usually not independent due to the geometric structures. For a checkerboard lattice,

it is reasonable to choose a unit cell with $4n$ local tensors T , $2n$ core tensors S , and $8n$ bond vectors λ , with n is an integer. Figure. S2 shows two examples of the unit cells with $n = 1$ and 2 . The PESS unit cell has a $\sqrt{2} \times \sqrt{2}$ structure for $n = 1$ [Fig. S2(a)] and has a 2×2 structure for $n = 2$ [Fig. S2(b)].

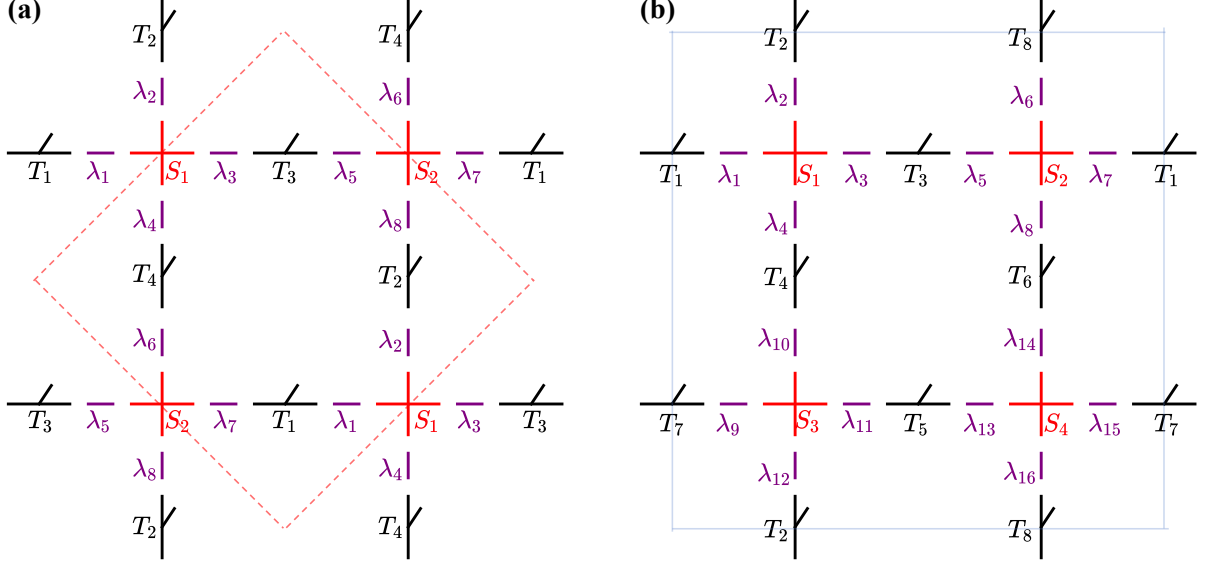


FIG. S2. The structure of the PESS unit cell on a checkerboard lattice. There are $4n$ local tensors T , $2n$ core tensors S , and $8n$ bond vectors λ in one unit cell (n is an integer). (a) Lattice constructed by the unit cell with $n = 1$. The structure is repeated with a $\sqrt{2} \times \sqrt{2}$ unit cell with the dashed red boundary lines; (b) the $n = 2$ unit cell with the thin blue boundary lines have a 2×2 structure. (The length of a J_2 bond is chosen as one lattice spacing)

Starting from an initial state $|\Psi_0\rangle$, either a random or a particular classical ordered configuration, an imaginary-time operation $\exp(-\delta\tau H)$ evolves the state to a convergent ground state as the iteration steps N increases. In practice, only operation on the local tensors are performed. Trotter-Suzuki approximation is used to decompose the global Hamiltonian H into local ingredient H_P on each plaquette:

$$\exp(-\delta\tau H) = \prod_P \exp(-\delta\tau H_P) + O(\delta\tau^2), \quad (\text{S2})$$

where H_p is the local Hamiltonian with spin operator S_i on i ($i = A, B, C, D$) (Fig. S1) and expressed as

$$H_P = J_1(S_A \cdot S_B + S_B \cdot S_C + S_C \cdot S_D + S_D \cdot S_A) + J_2(S_A \cdot S_C + S_B \cdot S_D). \quad (\text{S3})$$

Using the tensor network state $|\Psi\rangle$ with convergent T , S , and λ , the physical properties, e.g., bond energy, can be calculated through

$$\langle O \rangle = \langle \Psi | O | \Psi \rangle / \langle \Psi | \Psi \rangle, \quad (\text{S4})$$

where O is any local operator. We evaluate it using a real space coarse-graining procedure known as the corner transfer matrix renormalization group (CTMRG) [S2, S3] which enables one to reach the thermodynamic limit. The results are convergent with the truncation dimension of the CTMRG step larger than D^2 .

BENCHMARK RESULTS

We first use a $\sqrt{2} \times \sqrt{2}$ unit cell with four local tensors T ($n = 1$) with the virtual bond dimension $D = 4$ form the tensors and set the time interval $\delta\tau = 0.02J^{-1}$. The comparison between the PESS results of the Heisenberg interaction on the checkerboard lattice and previous results from other methods are listed in Table S1 at different J_1 and J_2 .

At $J_1 = 1, J_2 = 0$, the model reduces to a 2D Heisenberg model, the result of ground state energy at $D = 4$ in our PESS calculation is already consistent with the Density Matrix Renormalization Group (DMRG) [S4] and Monte Carlo

| (J_1, J_2) | PESS | Others |
|--------------|---------|-------------------|
| (1, 0) | -0.6683 | -0.6694 (DMRG,MC) |
| (1, 2) | -0.8965 | -0.876 (iPEPS) |
| (0, 1) | -0.4410 | -0.4410 (iTEBD) |

TABLE S1. Comparison of our calculated ground state energy per site at the thermodynamics limit with PESS and the results from other methods.

(MC) [S5] extrapolated results, and better than the results from many other methods [S6]. At $J_2/J_1 = 2$, The ground state energy of the nearly degenerate bond-centered charge correlated (BCC) and site-centered charge correlated (SCC) states obtained by PESS is lower than the energy of the stripe ordered phase from iPEPS calculation [S7]. At $J_1 = 0, J_2 = 1$, the checkerboard model is decoupled into independent 1D chains in two different directions. The result of PESS calculation is exactly the same with the infinite time-evolving block decimation (iTEBD) [S8] calculation with the same D and already consistent with the exact result $-\ln(2) + 1/4$. the equivalence between the PESS and the iTEBD is due to the reason that the simplex tensor S recover the geometric structure of the checkerboard lattice. At $J_1 = 0$, the simplex tensor S is the direct tensor product of two iTEBD Schmidt matrix λ of the two independent directions:

$$S'_{ij,kl} = \lambda_{i,k} \times \lambda_{j,l} \quad (\text{S5})$$

where $S'_{ij,kl}$ is the reshaped matrix form of the simplex tensor S_{ijkl} . Thus the simplex tensor can be constructed by two independent Schmidt matrices perpendicular with each other.

In principle, increasing the virtual bond dimension D (or Schmidt rank χ in 1D) can improve the results for any tensor network method. However, the choice of an ansatz following the geometric structure of the system can efficiently improve the calculation even at small D . With PESS on a checkerboard lattice, we obtain benchmark results of the ground state energies with $D = 4$. For the results shown in the main text, we use $D = 4$ with an 2×2 unit cell ($n = 2$ with eight local tensors) to compare the energies of different degenerate ground states (Fig. 2 in the main text) and use $D = 4$ with a $\sqrt{2} \times \sqrt{2}$ unit cell ($n = 1$ with four local tensors) to determine the phase transition boundaries (Fig. 3,4 in the main text).

DISCUSSION ON THE DEGENERATE BCC/SCC-TYPE STATES

Results in the XY -limit

The nearly degenerating behavior of the BCC/SCC-type states found in the main text also exists in the XY -limit. As shown in Fig. S3 for the degenerate states in the XY -limit, there is no significant difference from the results in the Heisenberg case, except that the magnitude of the bond energies in J_1 direction are relatively larger than those in the Heisenberg case, which indicates that the local bosonic wave-function spreads further for the XY case. This property is consistent with the fact that there is no density interaction in the XY -limit.

A new notation to classify the SCC states

In the nearly degenerate BCC/SCC-type phase, both the Néel* and the zigzag state have a 2×2 structure. We used (2×2) SCC and $(2 \times 2)'$ SCC to distinguish these two SCC states. Here, we show that the SCC states can be further classified by a combined nesting vector, i.e. $(x, y) \equiv [(x, \pi), (\pi, y)]$ (π stands for the bosons occupied on every other lattice spacing), representing the repeating patterns of the vertical (horizontal) lines of bosons in the horizontal (vertical) directions. For example, the surprising zigzag state is labeled as $(0, \pi)$ (abbr. of $[(0, \pi), (\pi, \pi)]$) with the vertical lines of bosons repeat themselves every lattice spacing horizontally and horizontal lines repeat every other lattice spacing vertically (Fig. S4). Similarly, the stripe (Néel* state) is labeled by (π, π) $[(0, 0)]$. The other degenerate states with all the possible combination of (x, y) can be obtained if the size of the unit cell is further increased.

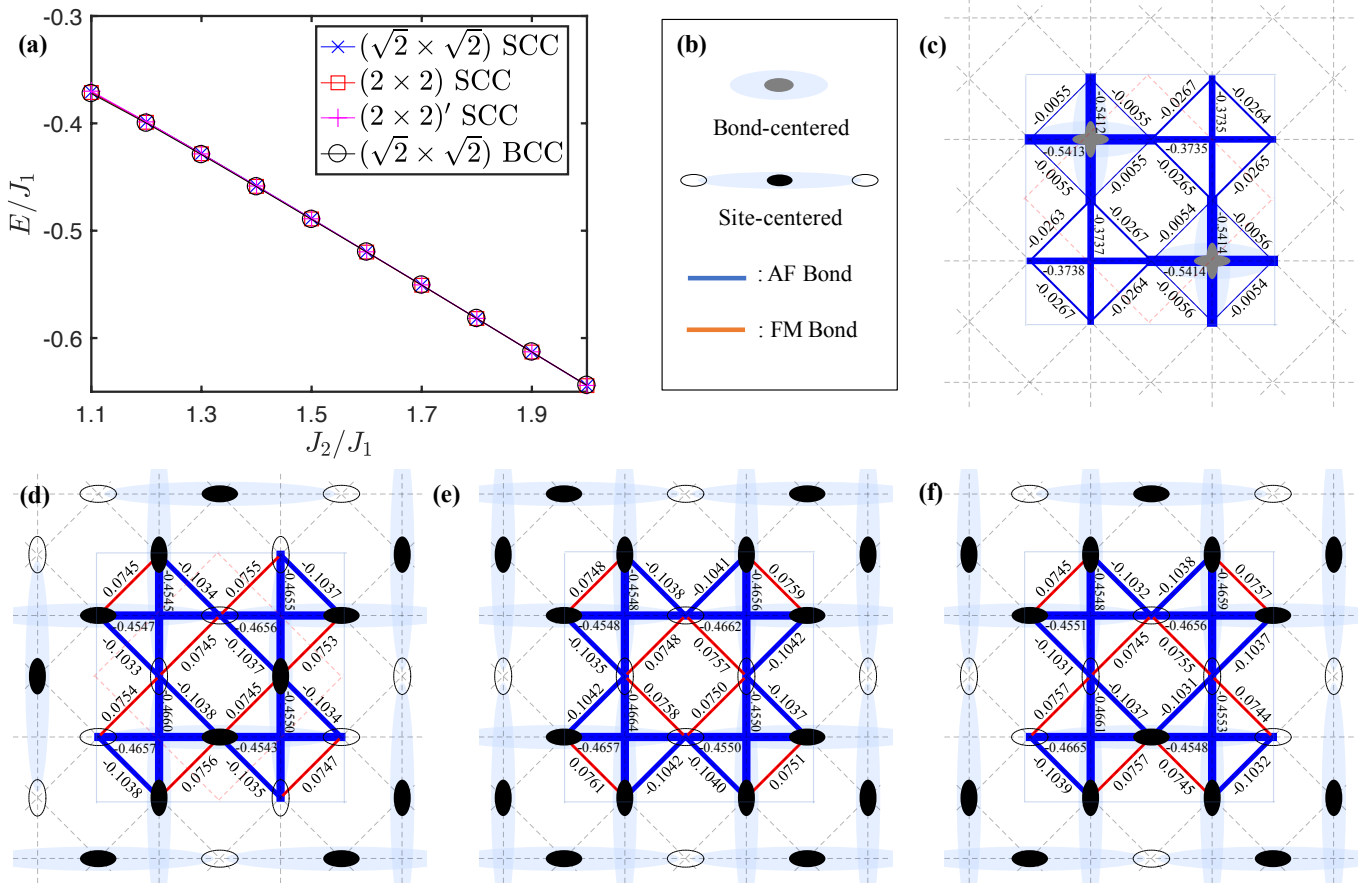


FIG. S3. Nearly degenerate ground state energies of checkerboard model at the XY-limit at $J_2 > J_1$, notations are the same with those in Fig. 2 of the main text. (a) Energies of different states with different J_2/J_1 . (b) Symbols used in (c-f) are illustrated. (c-f) Examples of the different energy bond configurations at $J_2/J_1 = 1.5$ are shown (a PESS unit cell is bounded by the light blue box): (c) $(\sqrt{2} \times \sqrt{2})$ BCC (crossed-dimer), (d) $(\sqrt{2} \times \sqrt{2})$ SCC (stripe), (e) (2×2) SCC (Néel*), and (f) $(2 \times 2)'$ SCC (zigzag). In (c,d), one period of the charge order is bounded by the dashed red lines. In (e,f), the period is the same with the PESS unit cell.

Discussion on the higher energy states from the bosonic picture

We have shown that the nearly degenerate ground states can be interpreted by the bosonic picture. In all the SCC states, the bosons are occupied every other sites in the horizontal or vertical orbital directions (two J_2 bond directions). Meanwhile, there are two different types of J_1 bonds for each boson with equal probability: one is connect to a hole, the other is connect to another boson. In the BCC state, the crossed-dimer configuration is formed by two bosons in different orbital direction moving into the same plaquette with J_2 interactions. In this configuration, there are also two different types of J_1 bonds: one is the bonds inside the crossed-dimer plaquette, the other is those in between different crossed-dimer plaquette. Thus, the bond asymmetry is also appear in each J_1 direction.

To further illustrate the efficiency of the bosonic interpretation, we discuss the higher energy states. For a SCC state, moving a boson to a hole, either through J_1 or J_2 bond will generate a configuration with two bosons connected by a J_2 bond [Fig. S5(a)], where the local wave-function of the two bosons overlap with each other, which result in a higher energy state. For the BCC case, beside the crossed-dimer state, a Shastry-Sutherland (SS) like dimer configuration [Fig. S5(b)] is another possible state where there is no overlap of bosonic wave-functions in the same J_2 orbital direction. This state is corresponding to the case when each boson is located at the center of each plaquette with J_2 interactions. However, different from the crossed-dimer BCC state where there are two different J_1 bonds, the J_1 bonds in the SS dimer state are all the same. They are all inter-dimer bonds and forming pairs of bonds connect to a common dimer [two red lines in Fig. S5(b)], which also generate some overlap of the local wave-functions between bosons and result in a higher energy state.

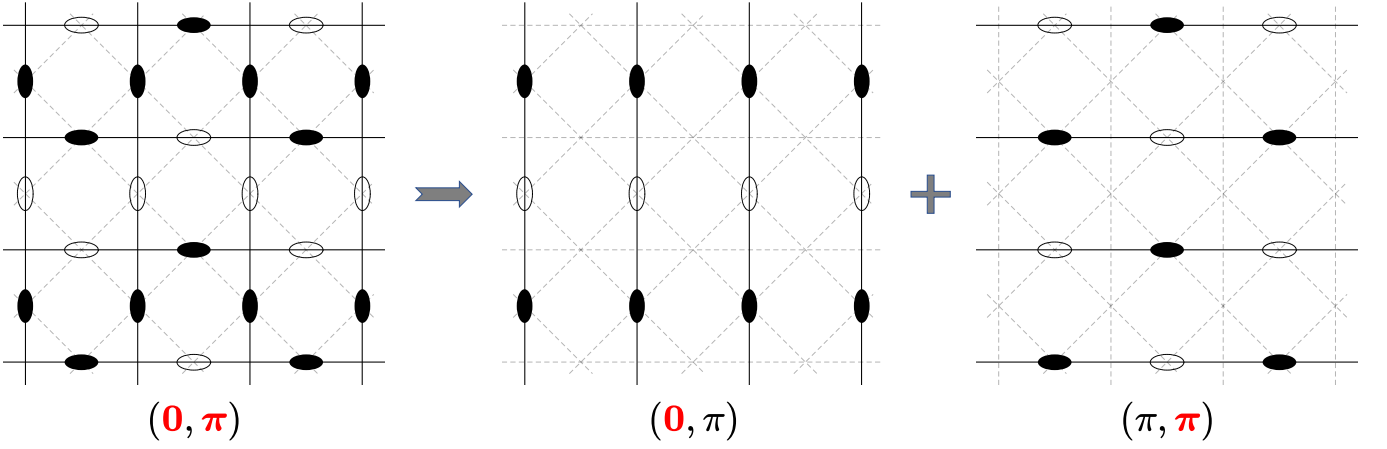


FIG. S4. A new notation to classify the SCC state for the zigzag state. The charge density patterns on a checkerboard lattice can be represented by the charge patterns in two different directions. In each direction, the charge is occupied at every other sites, labeled by a black π in the nesting vector. The repeating pattern of the charge chain in the perpendicular direction is labeled by the red value. E.g., 0 stands for the chain is repeated every lattice spacing.

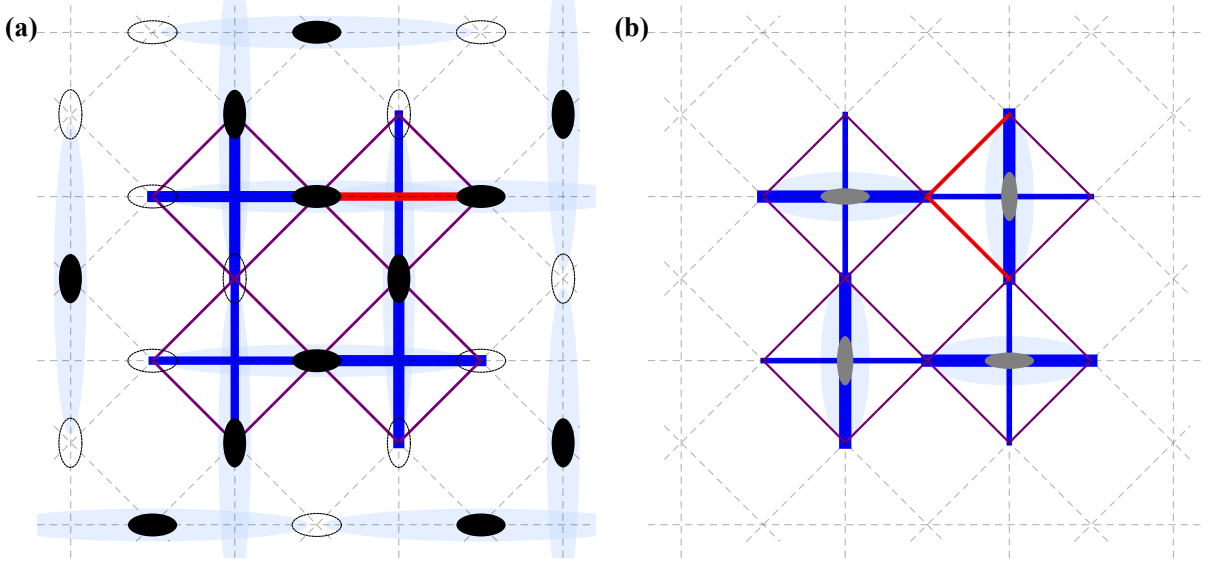


FIG. S5. Examples of higher energy states. (a) The configuration of a higher energy SCC state with two bosons are neighbors connected by a red line in the horizontal direction. (b) The SS configurations (a higher energy BCC state). The two red lines show the two nearest neighbor bonds shared by the same dimer.

THE META-STABLE CDW STATE IN THE XY -LIMIT

At $J_2 \sim J_1$, we find a meta-stable CDW state in the XY -limit. To illustrate the difference between the Heisenberg and the XY -limit, we start from a classical Néel configuration and evolve the state iteratively for both limits. Figure S6 shows the energy with a function of the evolution step N . For the Heisenberg limit, it goes monotonous to the P-VBS ground state. However, for the XY -limit, a meta-stable CDW state with a remaining AF ordered feature in the z direction exist before it goes to the paramagnetic ground state.

The CDW state in the XY -limit can be understood in the bosonic picture. In the $J_1 \gtrsim J_2$ region, the kinetic hopping along the J_1 and J_2 bond directions give opposite sizes of the same configuration with bosons occupied in the neighbor sites along J_1 directions in the wave-function (Fig. S7). This frustration behavior decouples two charge ordered states and breaks the symmetry of these two degenerate states to a CDW state.

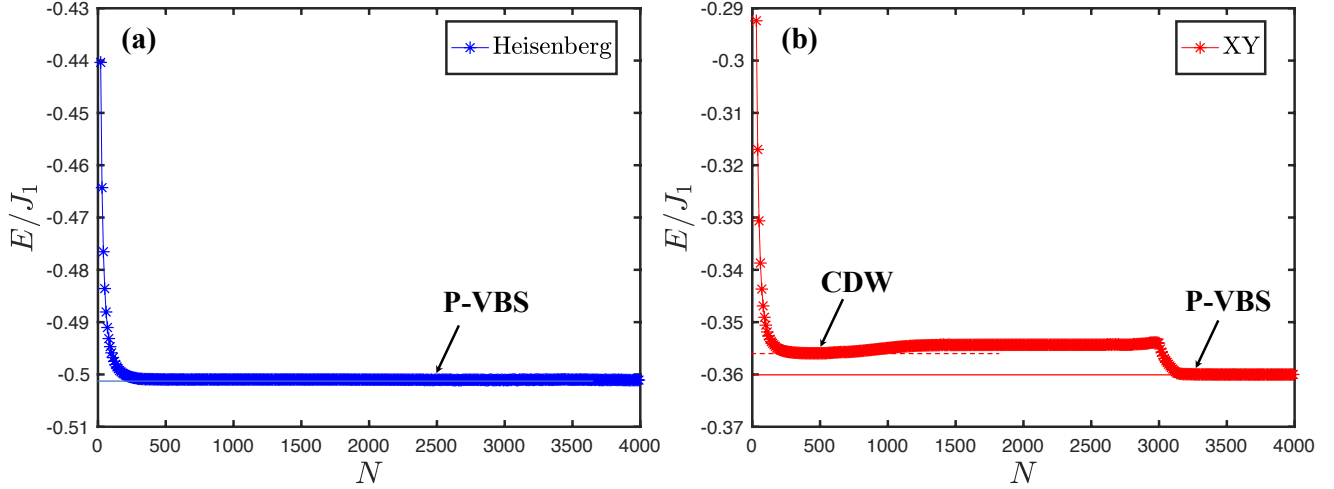


FIG. S6. The energy per site at $J_2/J_1 = 0.99$ as a function of the time evolution step (N) is shown. Starting from a classical Néel configuration, the system is evolved upto 4000 times and the energy is calculated at every ten steps. The energy ranges shown in both the Heisenberg and the XY cases are taken as $0.08J_1$. (a) In the Heisenberg limit, the state goes monotonous to the ground state, a P-VBS state (thin blue line). (b) In the XY -limit, before ended at the P-VBS state (the solid thin red line), the state first evolves to a meta-stable CDW state (dashed thin red line).

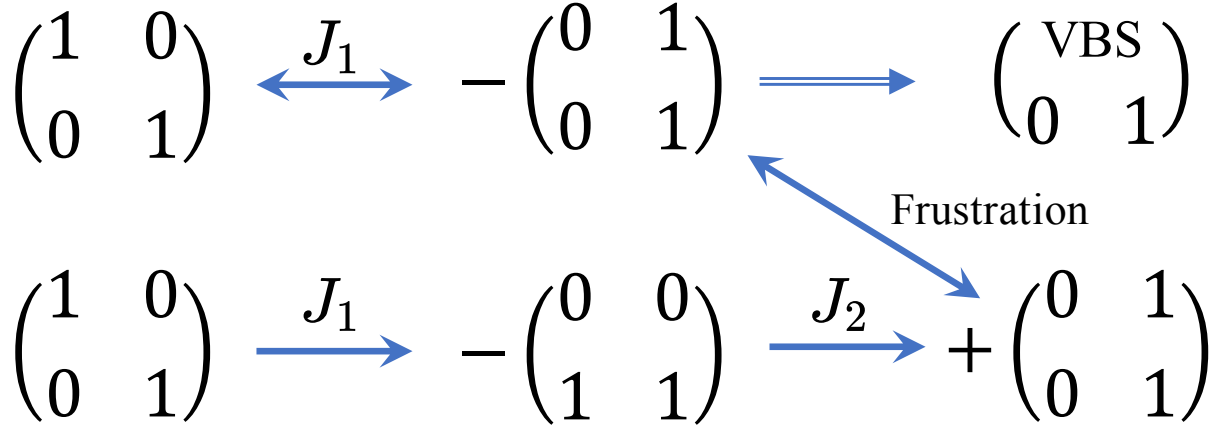


FIG. S7. The frustration due to the hopping at the J_1 and J_2 direction is illustrated in the configuration of one plaquette, where 1 and 0 stand for a boson and a hole, respectively.

DISCUSSION ON P-VBS STATES

In the P-VBS state region, the plaquettes may sit either on the squares with or without J_2 bonds. The energies of both cases are lower than those of AF ordered configuration and the J_2 -direction BCC/SCC-type configurations. In the isotropic limit ($J'_1/J_1 = 1$) and at $J_2 \sim J_1$, the PESS calculation favors the plaquette configurations on the squares with J_2 bonds. Figure S8(a) shows an example at $J_2 = J_1$. However, in the wide region of the P-VBS state with the nematic perturbation $J'_1 \neq J_1$, the PESS calculation favors the configuration without J_2 bonds in the plaquette. Figure S8(b) shows an example at $J'_1/J_1 = 0.9$, $J_2/J_1 = 0.8$. The interplay between the two configurations inside the P-VBS state region deserves a future study with further modifying the PESS ansatz to fit both the plaquette and the J_2 crossing geometries. For example, constructing the simplex tensor S on the plaquette without J_2 bonds and a four-virtual-leg local tensor T in the PESS wave-function ansatz with a selected symmetric time evolution update scheme H_p on all the plaquette (with and without the J_2 bonds) may provide a possible method to favor all the configurations of the P-VBS states.

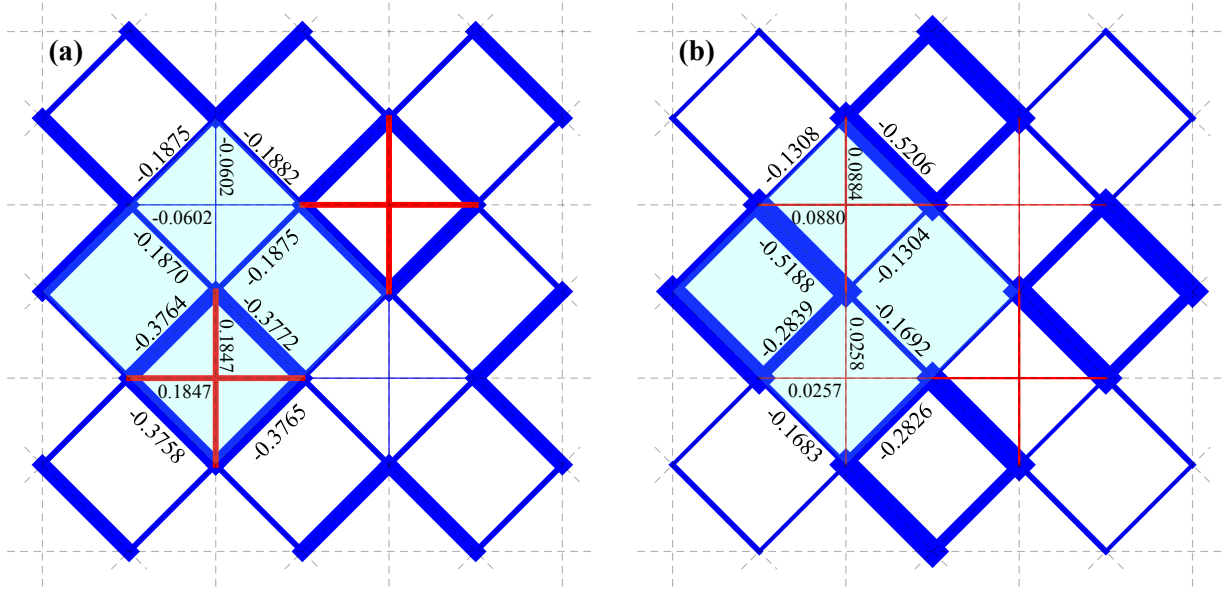


FIG. S8. Energy configurations for P-VBS states. (a) Example of the plaquettes on the squares with J_2 bonds at $J_1'/J_1 = 1$, $J_2/J_1 = 1$. (b) Example of the plaquettes on the squares without J_2 bonds at $J_1'/J_1 = 0.9$, $J_2/J_1 = 0.8$. The numbers show the bond energies and the thickness of each bond indicates the magnitude. The green regions represent a $\sqrt{2} \times \sqrt{2}$ PECS unit cell.

* wlzouhy@sjtu.edu.cn

† weiku@sjtu.edu.cn

- [S1] Z. Y. Xie, J. Chen, J. F. Yu, X. Kong, B. Normand, and T. Xiang, Phys. Rev. X **4**, 011025 (2014).
[S2] T. Nishino and K. Okunishi, Journal of the Physical Society of Japan **65**, 891 (1996).
[S3] P. Corboz, J. Jordan, and G. Vidal, Phys. Rev. B **82**, 245119 (2010).
[S4] E. Stoudenmire and S. R. White, Annual Review of Condensed Matter Physics **3**, 111 (2012).
[S5] A. W. Sandvik, Phys. Rev. B **56**, 11678 (1997).
[S6] E. Manousakis, Rev. Mod. Phys. **63**, 1 (1991).
[S7] Y.-H. Chan, Y.-J. Han, and L.-M. Duan, Phys. Rev. B **84**, 224407 (2011).
[S8] G. Vidal, Phys. Rev. Lett. **98**, 070201 (2007).